NANO LETTERS

Letter

pubs.acs.org/NanoLett

What Does Annealing Do to Metal–Graphene Contacts?

Wei Sun Leong,[†] Chang Tai Nai,[‡] and John T. L. Thong*,[†]

[†]Department of Electrical and Computer Engineering, National University of Singapore, Singapore, Singapore 117583

[‡]Department of Chemistry, National University of Singapore, Singapore, Singapore 117543

Supporting Information

ABSTRACT: Annealing is a postprocessing treatment commonly used to improve metal–graphene contacts with the assumption that resist residues sandwiched at the metal–graphene contacts are removed during annealing. Here, we examine this assumption by undertaking a systematic study to understand mechanisms that lead to the contact enhancement brought about by annealing. Using a soft shadow-mask, we fabricated residue-free metal–graphene contacts with the same dimensions as lithographically defined metal–graphene contacts on the same graphene flake. Both cases show comparable contact enhancement for nickel–graphene contacts after annealing treatment signifying that removal of resist residues is not the main factor for contact enhancement. It is found instead that carbon dissolves from graphene into the metal at chemisorbed Ni– and Co–graphene interfaces and leads to many end-contacts being formed between the metal and the dangling carbon bonds in the graphene, which contributes to much smaller contact resistance.

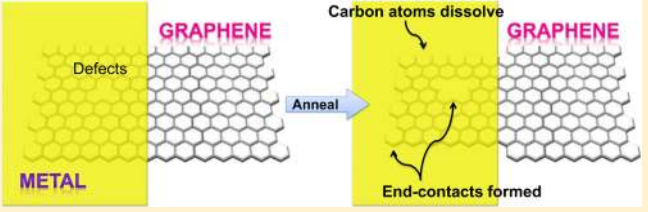

KEYWORDS: *Graphene, annealing, contact resistance, resist residues, soft shadow-mask, Raman analysis*

Contact resistance at the metal–graphene contacts has been recognized to be a significant impairment to the potential performance of graphene transistors. Recently, a number of approaches have been explored to address the issue of poor contacts such as gentle plasma treatment,[1,2] ultraviolet/ozone (UVO) treatment,[3,4] use of a sacrificial layer,[5] and annealing treatment.[1,6,7] The underlying principle of these approaches is to minimize resist residues that are left over at the source/drain contact regions of graphene devices by the lithography process. Out of these approaches, annealing treatment following a series of fabrication processes is the most common practice that has been adopted in many laboratories.[8−12] Although decomposition of resist residues takes place at temperatures higher than 200 °C,[9,13] the question is whether the resist residues sandwiched between the metal and graphene at the contacts can be removed by annealing because they had already been covered by thick metal film. Indeed, Chan et al. observed no significant changes to the contact resistance of their nickel-contacted graphene devices following annealing at 300 °C for 3 h.[10] On the other hand, Nagashio et al. found that the contact resistance of their resist-free nickel-contacted graphene devices that had been metallized by evaporation through a shadow mask is similar to that of resist-processed devices upon annealing.[8] More interestingly, to facilitate formation of covalent bonding between metal and graphene edges, annealing treatment plays an indispensable role where the graphene edges are defective[14] but is redundant for defect-free zigzag graphene edges.[15] All of these inconsistent observations give rise to the question of what annealing does to metal–graphene contacts to result in contact enhancement in most cases but insignificant changes under other circumstances.

In this paper, we attempt to close the gap in understanding. We report a novel technique to fabricate graphene devices with residue-free metal–graphene contacts, where nickel contact metallization is carried out by evaporation through a soft shadow-mask. Using this technique, we first fabricated graphene devices with both resist-patterned and residue-free nickel–graphene contacts to compare the impact of an annealing treatment. Unexpectedly, we found that annealing gives rise to comparable improvement in terms of contact resistance regardless of the presence of resist residues at the contacts. Consequently, we investigated the primary mechanism that leads to reduction of contact resistance in graphene devices as a result of annealing.

In order to compare the contact enhancement brought about by an annealing treatment, we fabricated on the same graphene strip exfoliated from Kish graphite an array of graphene back-gated field-effect transistors consisting of both resist-patterned and residue-free metal–graphene contacts. The device dimensions were kept the same throughout. Transistors with residue-free metal–graphene contacts were first fabricated on the freshly exfoliated strip, using a prepatterned PMMA soft shadow-mask as illustrated in Figure 1 (see Methods for details). Having protected these pristine contact areas with metallization, the transistors with resist-patterned contacts were then fabricated using a conventional electron beam lithography approach as described in Methods. The presence of resist residues on the graphene exposed to resist processes can be

Received: March 17, 2014
Revised: June 6, 2014
Published: June 9, 2014

ACS Publications © 2014 American Chemical Society

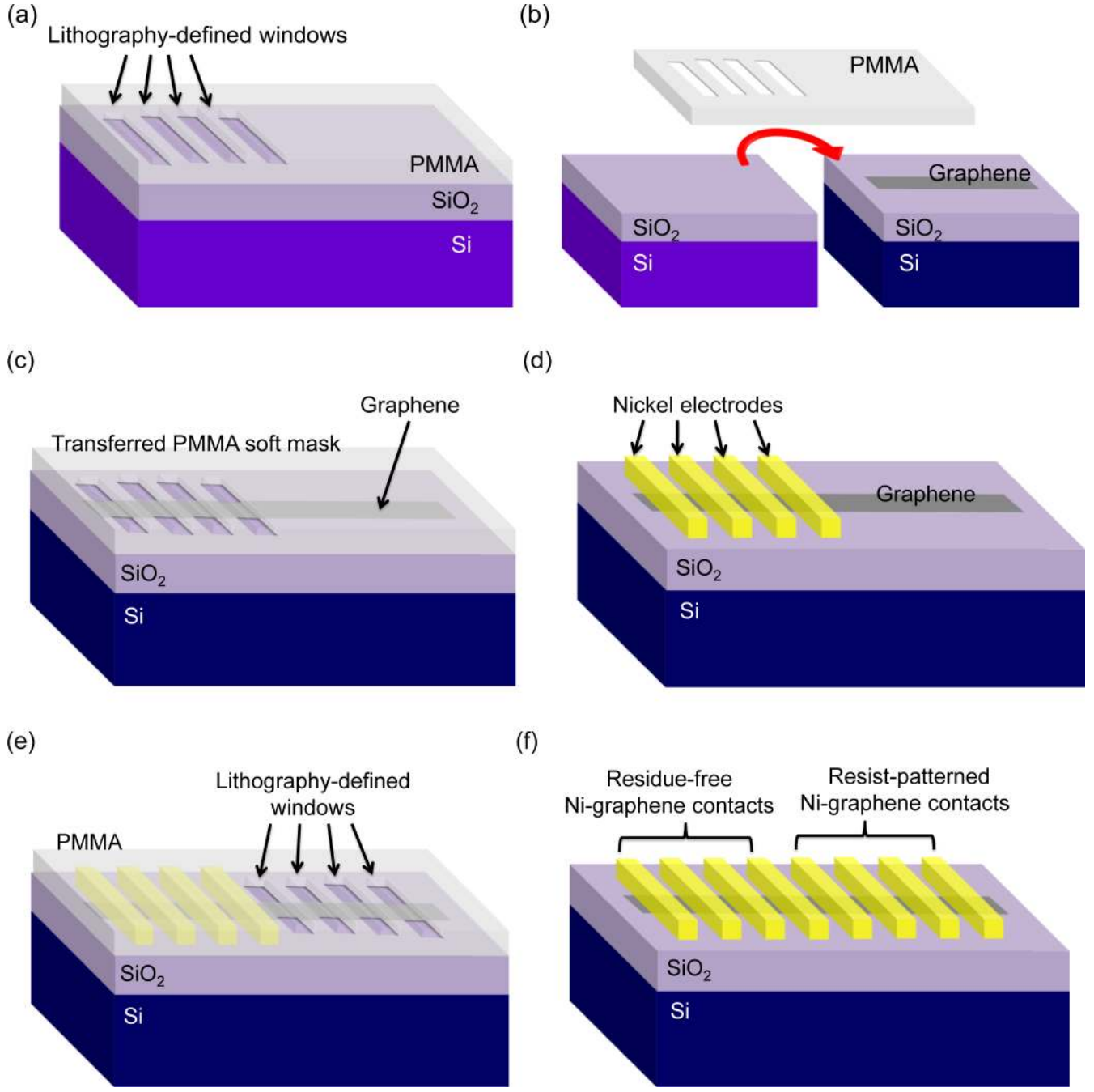

Figure 1. Schematics of the process showing the fabrication steps of a graphene transistor array consisting of both resist-patterned and residue-free metal–graphene contacts. (a) Four windows are created in the middle of the substrate using electron beam lithography (EBL). (b) The prepatterned PMMA film is peeled-off from the substrate using "Scotch-tape" technique and transferred onto another target substrate with freshly exfoliated graphene strip on it. (c) The EBL-opened windows are aligned to the exfoliated graphene in the desired direction with the help of a micromanipulator. (d) Thick Ni metallization is deposited as electrical contacts to the graphene device forming four residue-free metal–graphene contacts. (e) A layer of PMMA is spin-coated on the sample and EBL is used to delineate four metal contact windows on the graphene strip. (f) Thick Ni metallization is deposited as electrical contacts to the graphene device forming four resist-patterned metal–graphene contacts.

seen in the increased surface roughness of the graphene surface compared to that of the residue-free graphene contact area, both prior to metallization (Supporting Information Figure S1). This novel fabrication technique allows the residue-free contacts to have the same dimensions as the resist-patterned contacts as both of them were defined using electron beam lithography. In fact, the transferred PMMA shadow-mask can also be used directly as an electron beam resist layer for the subsequent patterning. For fair comparison, the device dimensions were standardized for all transistors, where the channel length and contact length are 1 μm, while the channel width and contact width are 3 μm, being the natural width of the exfoliated graphene strip. For this study, the electrode material chosen is nickel as it is one of the chemisorbed metals that has been theoretically predicted to react with graphene strongly through orbital hybridization and appears to provide low contact resistance to graphene with the smallest variation.[12,15] Figure 2a shows a transistor array that contains

dx.doi.org/10.1021/nl500999r | Nano Lett. 2014, 14, 3840–3847

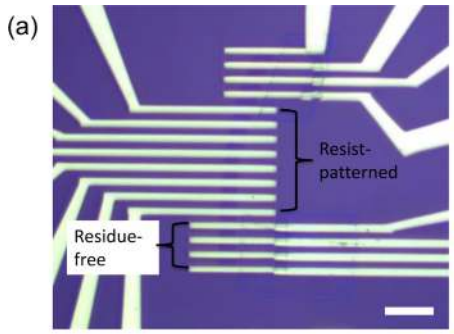

(b)

R_C taken at V_G = -20V (Ω•μm)	Resist-patterned	Residue-free
As-fabricated	581	567
Annealed	349	335

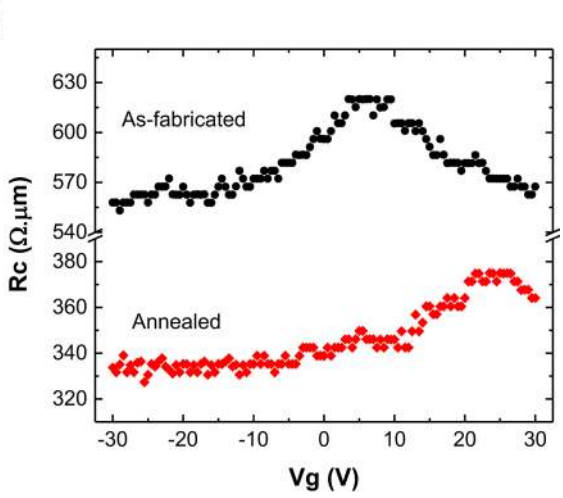

Figure 2. Comparison of contact enhancement by annealing at 300 °C for 1 h for graphene transistors that consist of both residue-free and resist-patterned metal–graphene contacts. (a) Optical image showing an array of graphene transistors containing both residue-free and resist-patterned metal–graphene contacts. Scale bar: 10 μm. (b) The average contact resistance values (when back gate voltage = −20 V) for both residue-free and resist-patterned Ni-graphene contacts fabricated using the same graphene flake prior to and following 1 h of 300 °C annealing. (c) Contact resistance of a typical graphene transistor with residue-free Ni–graphene contacts as a function of applied back gate voltage. Similar trend was observed for graphene devices with resist-patterned metal–graphene contacts.

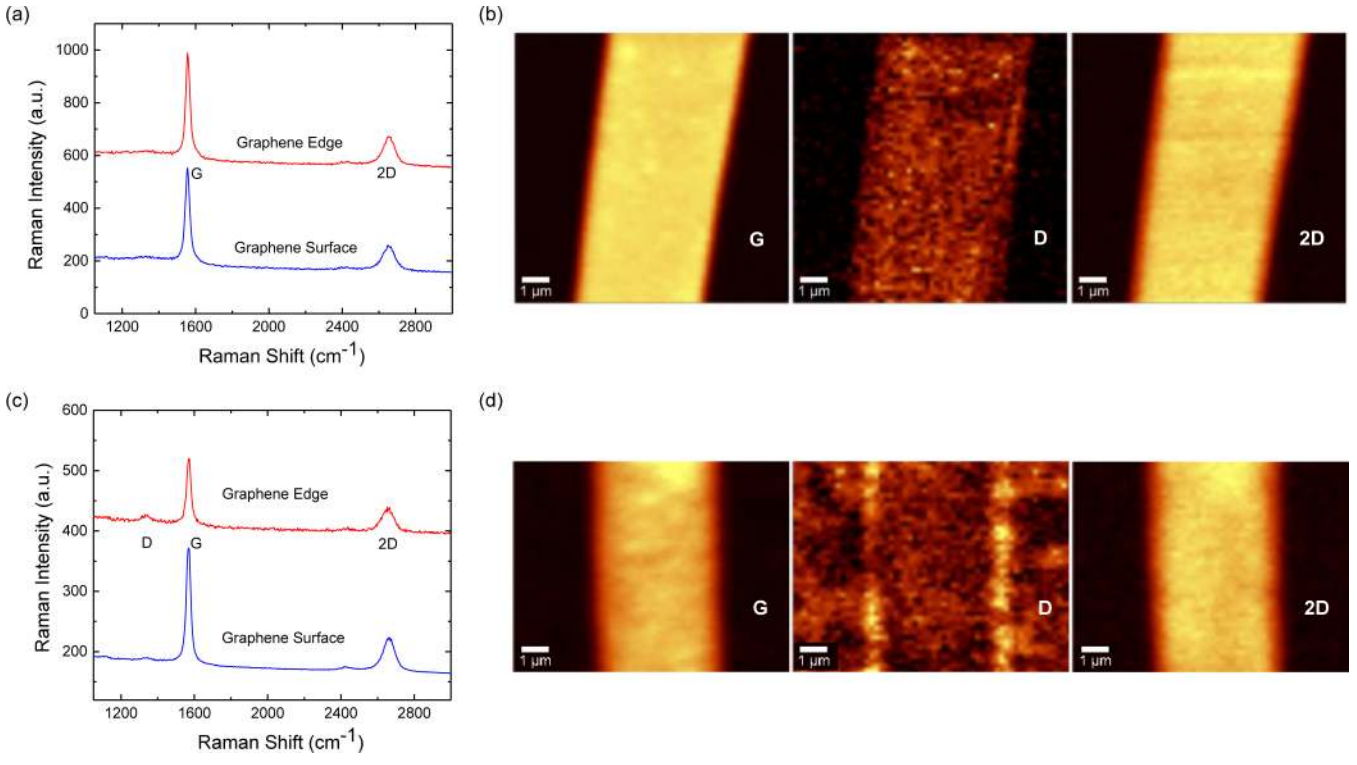

Figure 3. A piece of exfoliated few-layer graphene (three layers) was covered with a 100 nm thick of Ni film for more than 24 h at room temperature followed by acid dip to remove the Ni film. (a) Raman spectra taken at the graphene edge and surface. (b) Raman maps showing intensity of the G-, D- and 2D-band of the graphene flake. Subsequently, a Ni film was deposited on the same graphene flake again but the sample was annealed at 300 °C for 1 h this time followed by removal of the Ni film. (c) Raman spectra taken at the graphene edge and surface again. (d) Raman maps showing intensity of the G-, D- and 2D-band of the graphene flake.

both resist-patterned and residue-free contacts. Figure 2b summarizes the average contact resistance values for both resist-patterned and residue-free contacts fabricated using the same graphene flake prior to and following 1 h of 300 °C annealing treatment. Four-probe measurement technique was adopted to extract contact resistance of each graphene device via eq 1

$$R_C = \frac{1}{2}(R_{2p} - R_{4p})W \quad (1)$$

where R_C is the contact resistance, R_{2p} is the device's two-point resistance, R_{4p} is the device's four-point resistance, and W is the contact width. Electrical measurements for all devices were conducted in a high vacuum chamber and R_C was taken when

dx.doi.org/10.1021/nl500999r | Nano Lett. 2014, 14, 3840–3847

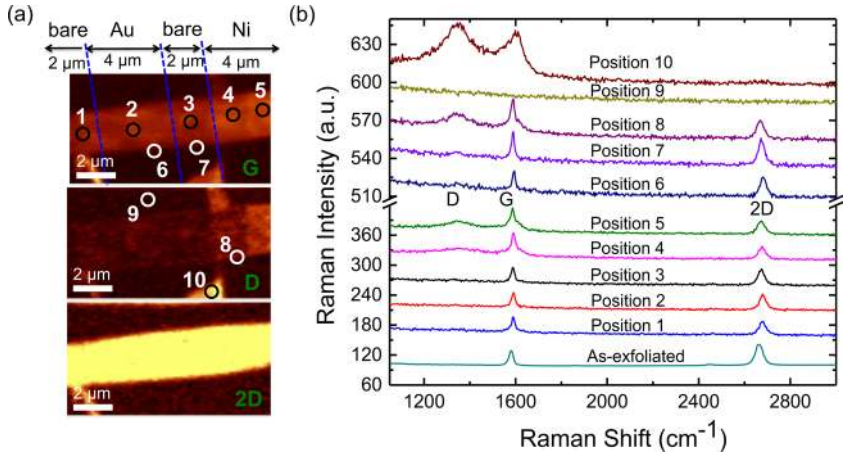

Figure 4. Comparison study of the annealing effect on both chemisorbed (Ni) and physisorbed (Au) metal–graphene interfaces. (a) Raman maps showing the intensity of G-band, D-band, and 2D-band of a processed exfoliated monolayer graphene. During the annealing process, parts of the graphene were covered by either Ni or Au strips (4 μm wide, 100 nm thick), as labeled in the G-band intensity map. (b) Raman spectra taken at different positions as indicated in (a).

the back gate voltage, V_{gs} = −20 V, in a regime where the R_C has insignificant gate dependence (Figure 2c). As can be seen from Figure 2b, both sets of transistors with resist-patterned and residue-free contacts have similar R_C values as-fabricated. More importantly, the average R_C for both sets of transistors improves by a similar factor after the annealing treatment. This observation suggests that the main contributing factor that leads to the contact enhancement as a result of annealing is not the removal of resist residues sandwiched at the metal–graphene contacts.

As a result of this finding, we sought to uncover the key mechanism that could account for why annealing improves metal–graphene contacts. Through Raman analysis, we examined the impact of annealing on the graphene that is covered by a thick metal film. A film of nickel (100 nm) was first deposited on a flake of freshly exfoliated few-layer graphene. The nickel film was left on the graphene sample for more than 24 h at room temperature (~25 °C), then the nickel film was removed by dipping into acid (concentrated HCl/HNO_3 3:1) for less than 5 min. Atomic force microscopy was used to ensure that the Ni film has been removed completely. Figure 3a shows Raman spectra of the processed graphene surface and its edges, while Figure 3b presents the Raman intensity maps of G-, D- and 2D-bands of the graphene flake. As can be seen, the processed graphene has uniform Raman signatures throughout the flake with negligible D-band signal. This implies that the processed graphene flake remained intact after nickel deposition and removal and, moreover, its edges are of pure zigzag configuration. Subsequently, a film of nickel (100 nm) was deposited on the same graphene flake again but the sample was annealed at 300 °C for 1 h this time followed by removal of the nickel film. As shown in Figure 3c,d, a clear D-band signal is observed at the graphene edges while it is negligible for the graphene surface. The emergence of disorder-induced Raman signature (D-band signal) at the graphene edges suggests that an annealing treatment alters both atomic arrangement and electronic properties of the graphene covered by nickel. Moreover, the modification tends to initiate from edges of the exfoliated graphene flake, rather than throughout the graphene flake. This is not surprising as the interior of the graphene is composed of sp^2-hybridized carbon–carbon bonds and hence is inert, while the graphene edges are more reactive and susceptible to bonding with other materials due to the presence of dangling bonds.

One possible mechanism that can give rise to the disorder-induced Raman signature for the annealed nickel-on-graphene sample presented above is the carbon dissolution–precipitation mechanism whereby carbon atoms from the graphene dissolve into nickel and precipitation of nickel carbides takes place at the same time. The broken carbon–carbon bonds in the graphene contribute to the emergence of the D-band signal captured by Raman spectroscopy. Dissolution of carbon requires initiation sites such as defects or dangling bonds in graphene, which exist along the edges of the exfoliated graphene and rarely in the basal plane but can be anywhere throughout the CVD-grown graphene because of its imperfect lattice and grain boundaries. The proposed mechanism here is supported by an earlier X-ray photoelectron spectroscopy (XPS) study that discovered a significant amount of nickel carbides formed after the nickel-contacted CVD-grown graphene had been vacuum annealed at 100 °C for 1 h.[16] On the basis of this carbon dissolution–precipitation mechanism, the carbon–carbon bond breaking in graphene results in many dangling carbon bonds along the periphery of the undissolved graphene and these dangling carbon bonds are expected to directly bond to the metal in end-contacted geometry[17] rather than the surface-contacted geometry, which is planar and usually obtained by putting metal on top of a graphene sheet. An XPS study was conducted on the annealed nickel-on-graphene sample to confirm the presence of nickel–carbon compound (see Supporting Information S2 for details). More importantly, end-contacted metal–graphene contacts have been theoretically predicted[18] and experimentally proven[19] to provide much smaller R_C for graphene devices compared to those based on the surface-contacted configuration. In brief, this provides a consistent explanation as to how the annealing process improves the R_C of graphene devices.

Nevertheless, formation of end-contacted metal–graphene contacts arising from the carbon dissolution–precipitation process is not applicable to all metals. Metals are divided into two groups when they are in contact with graphene: chemisorbed and physisorbed.[20,21] Strong interaction is predicted to occur at the chemisorbed metal–graphene interfaces such as Ti–, Co–, Ni– and Pd–graphene interfaces,

dx.doi.org/10.1021/nl500999r | Nano Lett. 2014, 14, 3840–3847

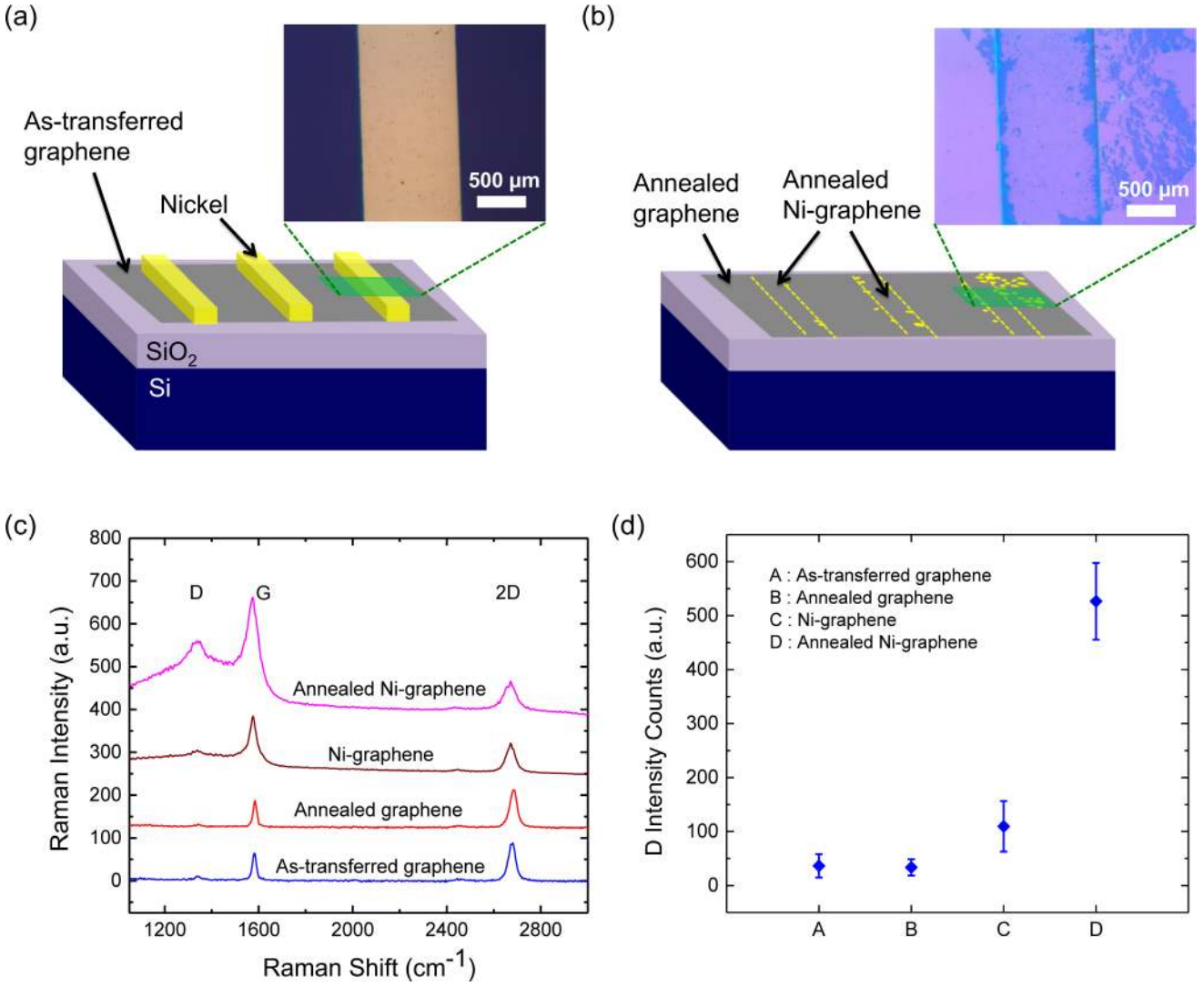

Figure 5. Investigation of the annealing effect on Ni-contacted monolayer CVD-grown graphene. (a) Schematic of the sample after annealing, showing several Ni bars deposited on the CVD graphene on a p^+ Si/SiO_2 substrate. Inset: Optical image of a Ni bar (1 mm wide, 100 nm thick) after 1 h of 300 °C annealing. (b) Schematic of the sample after Ni removal by acid, showing the CVD graphene on a p^+ Si/SiO_2 substrate with some residual nickel-carbon compound. Inset: Optical image of the marked region. (c) Raman spectra of the CVD graphene sample taken at different positions as indicated. (d) D-peak intensity counts summed over 3600 spectra for four different types of sample as indicated.

whereas physisorbed interfaces such as Au− and Pt−graphene interfaces are bonded weakly. Furthermore, transition metals such as Au with completed d-orbital shell are unlikely to react with carbon even if they were annealed together.[22] In Figure 4, we compare the annealing effect for both chemisorbed (Ni) and physisorbed (Au) metal−graphene interfaces that were fabricated on the same exfoliated graphene flake. The freshly exfoliated graphene flake has a 2D-band signal with full width at half-maximum (fwhm) of 35.6 cm^{-1}, showing that it is a monolayer graphene (Figure 4b). Both Au and Ni strips (100 nm thick, 4 μm wide) were thermally evaporated on the monolayer graphene as indicated in Figure 4a. Subsequently, the sample was annealed at 300 °C for 1 h followed by 5 min acid dip (concentrated HCl/HNO_3 3:1) to remove both metal films concurrently. Figure 4b shows the Raman spectra of the processed graphene taken from some representative positions as indicated in Figure 4a. As expected, the graphene portion covered by Au (Position 2) remains intact following annealing and has a Raman spectrum that is similar to that of the exposed graphene portion (Positions 1 and 3). In contrast, the graphene portion covered by Ni (Positions 4 and 5) is no longer intact following annealing and shows increased and nonuniform D-band signal. Consistent results were observed if we compare along the graphene edges (Positions 6, 7, and 8). The graphene edges covered by Ni (Position 8) show significant D-band signal, while the signal is negligible for both the graphene edges of the exposed portion (Position 7), and the Au-covered portion (Position 6). Furthermore, for the graphene portion covered by Ni, a tiny hump was observed throughout the graphene surface at ∼1350 cm^{-1}, which is the characteristic location of D-band signal of graphene. It is worth noting that the Raman spectrum of nickel−carbon compound consists of two broad characteristic peaks at ∼1350 and ∼1590 cm^{-1}, which are very close to the D- and G-peaks' position of graphene.[23,24] Therefore, the slight increase of D-band signal for the graphene portion covered by Ni (Position 4) compared to the exposed graphene portion (Position 3) can be attributed to the presence of a small amount of the nickel−carbon compound. Moreover, a new feature was detected at Position 10, which had no graphene initially, and is confirmed to be

dx.doi.org/10.1021/nl500999r | Nano Lett. 2014, 14, 3840−3847

nickel−carbon compound from its Raman spectrum as it consists of only the latter's two broad characteristic peaks. In contrast, no characteristic Raman peak was observed from the Au-covered blank substrate portion (Position 9). As for the nonuniform Raman signal observed at the graphene portion covered by Ni (Positions 4 and 5), we attribute it to the formation of nickel−carbon compound on the graphene surface that initiates at random locations. There is also the possibility of the nickel−carbon compound being redeposited randomly on the sample as a result of the wet chemical process (metal etching by acid); for example, Position 10, which was not covered by any metal film, shows a clear nickel−carbon compound Raman signature (Supporting Information S3). Besides that, we repeated this experiment on an exfoliated few-layer graphene and similar results were observed (Supporting Information S4). To sum up, the Raman results indicate that the proposed carbon dissolution−precipitation mechanism during annealing only applies to Ni−graphene interfaces but not for Au−graphene interfaces. In addition, we found that the R_C of Au-contacted graphene devices drops by only 3% for resist-patterned contacts and 1% for residue-free contacts upon an annealing treatment (see Supporting Information S5 for details). Apart from that, we also investigated Co-contacted-graphene through Raman analysis (Supporting Information S6) and, notably, its Raman spectrum undergoes similar changes as with the Ni-contacted graphene. These results provide additional support evidence to show that the carbon dissolution−precipitation mechanism applies to chemisorbed metal−graphene interfaces such as Ni− and Co−graphene interfaces, but not to Au−graphene interfaces that are physisorbed.

Although it has been shown that the carbon dissolution process takes place spontaneously upon metal deposition on CVD-grown graphene,[17] such metal−graphene chemical reaction is expected to be more pronounced at higher temperatures and hence lead to the improved metal−graphene contacts. In Figure 5, we demonstrate that annealing can substantially enhance the nickel−graphene chemical reaction in CVD-grown graphene compared to the spontaneous reaction at room temperature. Figure 5a,b illustrates the sample preparation steps for this study. Monolayer CVD-grown graphene on p-doped silicon substrates with 285 nm of oxide thickness was purchased from Graphene Laboratories Inc. Several Ni bars (1 mm wide, 100 nm thick) were evaporated on the CVD graphene (Figure 5a) followed by 1 h of annealing at 300 °C. The sample was then dipped into acid to remove the nickel (Figure 5b). For comparison purposes, another sample was prepared using the same approach but without annealing. The Raman spectra taken at different positions on the graphene sample are shown in Figure 5c. The fwhm of the 2D-band for as-transferred CVD graphene is 34.87 cm^{-1} and the D/G peak intensity ratio is 0.15, indicating that it is of single layer with a certain amount of defects. For "annealed graphene", which was not covered by Ni during annealing, its 2D peak has a fwhm similar to that of the as-transferred graphene (34.51 cm^{-1}) and smaller D/G peak intensity ratio (0.11). This signifies that the annealing process improved the quality of graphene. On the other hand, the "annealed Ni−graphene", which represents the graphene portion that was capped by Ni bars during annealing, has a much broader 2D peak (fwhm = 66.18 cm^{-1}) and significantly larger D/G peak intensity ratio (0.77). The Raman spectrum of "Ni−graphene", which represents the graphene portion that was capped by Ni bars for more than 24 h at room temperature and taken from another sample where annealing was omitted, has a 2D peak with smaller fwhm (45.13 cm^{-1}) and much weaker D-band intensity compared to the "annealed Ni−graphene" sample. Additionally, the D-peak intensity counts summed over 3600 spectra for four different types of sample, which were extracted from a Raman mapping over an area of 10 × 10 μm^2 with ∼167 nm step size, are plotted in Figure 5d. The average D-peak intensity of the "annealed Ni−graphene" is at least 5 times stronger than that of the "Ni−graphene". In short, the results corroborate our hypothesis that the annealing treatment can dramatically enhance the metal−graphene chemical reaction and is consistent with our explanation of why R_C improves in graphene devices after a simple annealing treatment.

Nevertheless, extended annealing is unlikely to improve metal−graphene contacts owing to the limited amount of initiation sites in graphene for carbon dissolution to take place, even for CVD-grown graphene (see Supporting Information S7 for details). To investigate the impact of annealing duration on R_C, we fabricated 10 back-gated transistors using exfoliated graphene with resist-patterned Ni−graphene contacts using the conventional electron beam lithography approach as before (see Methods for details). For this series of devices, the channel length, channel width, contact length, and contact width are all 2 μm. Four-probe measurement technique was used to extract the R_C of each graphene device via eq 1. Electrical measurements were conducted in high vacuum at room temperature on this series of devices. The measured R_C at a carrier density of 7.5 × 10^{10} cm^{-2} is plotted in Figure 6 as a function of cumulative annealing duration. After the first electrical measurement, the devices were annealed in situ at 500 K for 2 h followed by a second electrical measurement. The electrical measurement and annealing processes were repeated on all devices up to 24 h of cumulative annealing duration. It was found that the measured R_C of all devices dropped by ∼17% after the first 2 h of annealing and shows negligible changes thereafter. This shows that the annealing treatment improves the metal−graphene contacts up to a certain extent only, which agrees well with our hypothesis. Thus, a short

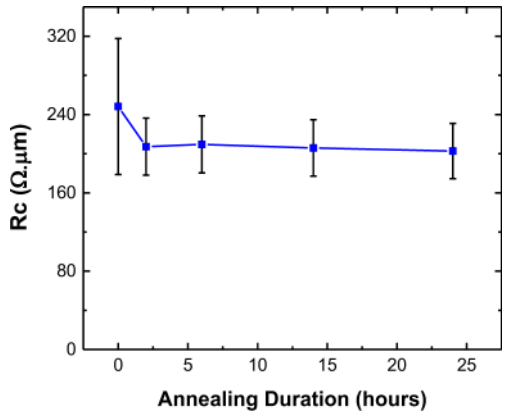

Figure 6. Measured contact resistance of 10 Ni-contacted graphene field-effect transistors at a carrier density of 7.5 × 10^{10} cm^{-2} (when V_{gs} = 1 V) as a function of the cumulative annealing duration. After the first electrical measurement, in situ 500 K anneal was performed on all devices for 2 h followed by the second electrical measurement at room temperature. The room-temperature electrical measurement and annealing processes were repeated on all devices up to 24 h of cumulative annealing duration.

dx.doi.org/10.1021/nl500999r | Nano Lett. 2014, 14, 3840−3847

annealing duration is sufficient to achieve similar improvement, which corroborates well with some prior works investigating contact enhancement achieved through rapid thermal annealing.[6,25]

In summary, annealing is a simple postprocessing technique often used to improve metal−graphene contacts although the achievable contact resistance remains far from satisfactory for graphene transistors. Utilizing a soft shadow-mask, we have been able to fabricate residue-free metal−graphene contacts with the same dimensions as those of the lithography-defined metal−graphene contacts. Similar contact enhancement was observed as a result of annealing for both residue-free and resist-patterned metal−graphene contacts ruling out the removal of resist residues upon annealing as the main reason for improved metal−graphene contacts. Through a series of studies, we showed that the key mechanism that leads to the contact enhancement upon annealing is the dissolution of carbon from graphene into metal at the chemisorbed metal−graphene interfaces such as Ni− and Co−graphene interfaces. Such metal−graphene chemical reaction results in the formation of strong chemical bonds between metal and the graphene edges, and hence provides a consistent explanation for the contact resistance improvement upon an annealing treatment. Limited by the amount of the dangling bonds and defects in graphene, extended annealing is unable to progressively improve the contact resistance to a significant extent. The understanding on how the annealing process improves the metal−graphene contacts presented in this work suggests that maximizing end-contact geometry between metal and graphene is the key approach to further improving the contact resistance in graphene devices.

Methods. *Fabrication of Both Resist-Patterned and Residue-Free Graphene Field-Effect Transistors on the Same Exfoliated Graphene Strip.* Graphene flakes were first exfoliated from Kish graphite on a SiO_2/p+ Si substrate with 285 nm of oxide thickness. A graphene flake of uniform width (3 μm) was selected for comparison study. To fabricate a soft shadow-mask, a 600 nm thick layer of poly(methyl methacrylate) (PMMA) was spin-coated on another SiO_2/p+ Si substrate and baked at 120 °C in an oven for 15 min. Four 20 μm × 1 μm windows were created in the middle of the substrate using electron beam lithography (EBL) followed by development in MIBK/IPA (1:3) (Figure 1a). The PMMA film was then peeled off from the substrate using a Scotch tape and transferred onto the targeted substrate with the freshly exfoliated graphene strip (Figure 1b). For this dry transfer technique, a micromanipulator was used to align the EBL-opened windows to the exfoliated graphene (Figure 1c). The sample with the soft mask was baked at 100 °C to improve adhesion. Subsequently, residue-free metal−graphene contacts were formed by evaporating 100 nm of Ni followed by lift-off in warm acetone (60 °C) for more than 12 h (Figure 1d). The sample was then spin-coated with a 600 nm thick layer of PMMA layer and baked at 120 °C in an oven for 15 min. After that, a number of resist-patterned metal−graphene contacts were delineated using EBL and metallized with 100 nm of Ni followed by lift-off (Figure 1f). All transistors were made from four-layer graphene and their dimensions were the same: the channel length and contact length were 1 μm and the channel width and contact width were 3 μm (Figure 2a). It is worth noting that the transferred PMMA soft mask could also be used directly as a resist layer for the subsequent patterning by EBL if so desired.

Annealing Process. All annealing processes for this study were conducted at 300 °C in a forming gas environment (400 sccm of 5% H_2 and 95% Ar at a total pressure of 10 Torr) for 1 h, unless otherwise specified. This annealing condition was chosen because annealing at 300 °C had been demonstrated to enhance the carrier mobility of graphene devices[26] and both forming gas and nitrogen provide the optimum annealing atmosphere.[6,25] The use of higher temperature is expected to be more effective in burning off resist residues that are left over from device fabrication processes, but temperatures higher than 300 °C should be avoided due to the increased coupling between a silicon dioxide substrate and the graphene.[26]

Raman Analysis. For this study, a Raman system (WITec alpha 300R) with a 532 nm laser excitation source and laser spot size of ∼320 nm was used. The laser power at the sample was always kept below 0.1 mW to avoid laser-induced heating.[27] All Raman mappings were conducted with a step size of 100 nm, unless otherwise specified.

■ ASSOCIATED CONTENT

Supporting Information

Comparison of the graphene surface between the residue-free and resist-patterned metal−graphene contacts prior to metallization, characterization of material composition of annealed nickel-on-graphene sample, verification of carbon dissolved from graphene into nickel, comparison study of the annealing effect on both Ni- and Au-contacted few-layer graphene, impact of annealing on Au-contacted graphene devices, Raman analysis of cobalt-contacted graphene, and investigation on the effect of extended annealing on Ni-contacted graphene. This material is available free of charge via the Internet at http://pubs.acs.org.

■ AUTHOR INFORMATION

Corresponding Author

*E-mail: elettl@nus.edu.sg.

Notes

The authors declare no competing financial interest.

■ ACKNOWLEDGMENTS

The authors would like to thank Mr. Zhao Xiangming for his fruitful discussion while brainstorming the idea of residue-free metal−graphene contacts. This project is supported by Grant R-263-000-A76-750 from the Faculty of Engineering, NUS and Grant NRF2011NRF-CRP002-050 from the National Research Foundation, Singapore.

■ REFERENCES

(1) Robinson, J. A.; LaBella, M.; Zhu, M.; Hollander, M.; Kasarda, R.; Hughes, Z.; Trumbull, K.; Cavalero, R.; Snyder, D. *Appl. Phys. Lett.* **2011**, *98* (5), 053103−1−053103−3.

(2) Choi, M. S.; Lee, S. H.; Yoo, W. J. *J. Appl. Phys.* **2011**, *110* (7), 073305−1−073305−6.

(3) Li, W.; Liang, Y.; Yu, D.; Peng, L.; Pernstich, K. P.; Shen, T.; Hight Walker, A. R.; Cheng, G.; Hacker, C. A.; Richter, C. A.; Li, Q.; Gundlach, D. J.; Liang, X. *Appl. Phys. Lett.* **2013**, *102* (18), 183110−1−183110−5.

(4) Chen, C. W.; Ren, F.; Gou-Chung, C.; Hung, S.-C.; Huang, Y. P.; Kim, J.; Kravchenko, I. I.; Pearton, S. J. *J. Vac. Sci. Technol. B* **2012**, *30* (6), 060604−060604−3.

(5) Hsu, A.; Wang, H.; Ki Kang, K.; Kong, J.; Palacios, T. *IEEE Electron Device Lett.* **2011**, *32* (8), 1008−1010.

(6) Balci, O.; Kocabas, C. *Appl. Phys. Lett.* **2012**, *101* (24), 243105−1−243105−5.

(7) Malec, C. E.; Elkus, B.; Davidović, D. *Solid State Commun.* **2011**, *151* (23), 1791−1793.
(8) Nagashio, K.; Ifuku, R.; Moriyama, T.; Nishimura, T.; Toriumi, A. In *Intrinsic Graphene/Metal Contact*; 2012 IEEE International Electron Devices Meeting (IEDM), San Francisco, California, United States, Dec. 10−13, 2012; pp 4.1.1−4.1.4.
(9) Gong, C.; Floresca, H. C.; Hinojos, D.; McDonnell, S.; Qin, X.; Hao, Y.; Jandhyala, S.; Mordi, G.; Kim, J.; Colombo, L.; Ruoff, R. S.; Kim, M. J.; Cho, K.; Wallace, R. M.; Chabal, Y. J. *J. Phys. Chem. C* **2013**, *117* (44), 23000−23008.
(10) Chan, J.; Venugopal, A.; Pirkle, A.; McDonnell, S.; Hinojos, D.; Magnuson, C. W.; Ruoff, R. S.; Colombo, L.; Wallace, R. M.; Vogel, E. M. *ACS Nano* **2012**, *6* (4), 3224−3229.
(11) Ifuku, R.; Nagashio, K.; Nishimura, T.; Toriumi, A. *Appl. Phys. Lett.* **2013**, *103* (3), 033514−1−033514−5.
(12) Nagashio, K.; Nishimura, T.; Kita, K.; Toriumi, A. *Appl. Phys. Lett.* **2010**, *97* (14), 143514−1−143514−3.
(13) Lin, Y.-C.; Lu, C.-C.; Yeh, C.-H.; Jin, C.; Suenaga, K.; Chiu, P.-W. *Nano Lett.* **2011**, *12* (1), 414−419.
(14) Smith, J. T.; Franklin, A. D.; Farmer, D. B.; Dimitrakopoulos, C. D. *ACS Nano* **2013**, *7* (4), 3661−3667.
(15) Leong, W. S.; Gong, H.; Thong, J. T. L. *ACS Nano* **2014**, *8* (1), 994−1001.
(16) Lahiri, J.; Batzill, M. *Appl. Phys. Lett.* **2010**, *97* (2), 023102−1−023102−3.
(17) Gong, C.; McDonnell, S.; Qin, X.; Azcatl, A.; Dong, H.; Chabal, Y. J.; Cho, K.; Wallace, R. M. *ACS Nano* **2013**, *8* (1), 642−649.
(18) Matsuda, Y.; Deng, W.-Q.; Goddard, W. A. *J. Phys. Chem. C* **2010**, *114* (41), 17845−17850.
(19) Wang, L.; Meric, I.; Huang, P. Y.; Gao, Q.; Gao, Y.; Tran, H.; Taniguchi, T.; Watanabe, K.; Campos, L. M.; Muller, D. A.; Guo, J.; Kim, P.; Hone, J.; Shepard, K. L.; Dean, C. R. *Science* **2013**, *342* (6158), 614−617.
(20) Giovannetti, G.; Khomyakov, P. A.; Brocks, G.; Karpan, V. M.; van den Brink, J.; Kelly, P. J. *Phys. Rev. Lett.* **2008**, *101* (2), 026803−1−026803−4.
(21) Khomyakov, P. A.; Giovannetti, G.; Rusu, P. C.; Brocks, G.; van den Brink, J.; Kelly, P. J. *Phys. Rev. B* **2009**, *79* (19), 195425−1−195425−12.
(22) Ōya, A.; Ōtani, S. *Carbon* **1979**, *17* (2), 131−137.
(23) Shi, J.; Nittono. *J. Mater. Sci.* **1996**, *15* (11), 928−930.
(24) Balaceanu, M.; Vladescu, A.; Braic, M.; Zoita, C. N.; Feraru, I.; Braic, V. *Optoelectron. Adv. Mater.* **2010**, *4* (12), 2167−2171.
(25) Chan Wook, J.; Ju Hwan, K.; Jong Min, K.; Dong Hee, S.; Sung, K.; Suk-Ho, C. *Nanotechnology* **2013**, *24* (40), 405301−1−405301−6.
(26) Cheng, Z.; Zhou, Q.; Wang, C.; Li, Q.; Wang, C.; Fang, Y. *Nano Lett.* **2011**, *11* (2), 767−771.
(27) Hao, Y.; Wang, Y.; Wang, L.; Ni, Z.; Wang, Z.; Wang, R.; Koo, C. K.; Shen, Z.; Thong, J. T. L. *Small* **2010**, *6* (2), 195−200.